A Modified Cable Formalism for Modeling Neuronal Membranes at High Frequencies

Claude Bédard and Alain Destexhe

Integrative and Computational Neuroscience Unit (UNIC), Centre National de la Recherche Scientifique, Gif-sur-Yvette, France

ABSTRACT   Intracellular recordings of cortical neurons in vivo display intense subthreshold membrane potential (V_m) activity. The power spectral density of the V_m displays a power-law structure at high frequencies (>50 Hz) with a slope of ~−2.5. This type of frequency scaling cannot be accounted for by traditional models, as either single-compartment models or models based on reconstructed cell morphologies display a frequency scaling with a slope close to −4. This slope is due to the fact that the membrane resistance is short-circuited by the capacitance for high frequencies, a situation which may not be realistic. Here, we integrate nonideal capacitors in cable equations to reflect the fact that the capacitance cannot be charged instantaneously. We show that the resulting nonideal cable model can be solved analytically using Fourier transforms. Numerical simulations using a ball-and-stick model yield membrane potential activity with similar frequency scaling as in the experiments. We also discuss the consequences of using nonideal capacitors on other cellular properties such as the transmission of high frequencies, which is boosted in nonideal cables, or voltage attenuation in dendrites. These results suggest that cable equations based on nonideal capacitors should be used to capture the behavior of neuronal membranes at high frequencies.

INTRODUCTION

One of the greatest achievements of computational neuroscience has been the development of cable theory (reviewed in (1,2)), and which can explain many of the passive properties of neurons, including how dendritic events are filtered by the cable structure of dendrites. Cable theory describes the space and time propagation of the membrane potential by partial differential equations. Such a formalism constitutes the basis of nearly all of today's computational models of dendrites, and is simulated by several publicly-available and widely-used simulation environments (reviewed in (3)).

Some experimental observations, however, may suggest that the standard cable formalism may not be adequate to simulate the fine details of dendritic filtering. One of these observations is the fact that the power spectral density (PSD) of synaptic background activity or channel noise does not match that predicted from cable theory (4–7). The PSD scales approximately as $1/f^\alpha$ with an exponent $\alpha = 2.5$, both for channel noise and background activity (Fig. 1, A and B), whereas cable theory would predict scaling with an exponent $\alpha = 4$ or $\alpha = 5$ for synaptic inputs distributed in dendrites ((5,8); see also Appendix 1), or $\alpha = 3.2$ to 3.4 when inputs are distributed in soma and dendrites (see Fig. 1, C and D). In other words, these data suggest that frequencies are filtered by dendritic structures in a way different from that predicted by traditional cable equations.

One possible origin of such a mismatch could be due to the fact that the permittivity of the membrane is frequency-dependent (9,10). However, capacitance measurements in bilipid membranes shows negligible variations at ~100 Hz

(see Fig. 5 in (10)), suggesting that the frequency-dependent model may not be the correct explanation for this range of frequencies. It could also be that distortions of the frequency-dependence arise from the complex three-dimensional morphology of the neuronal membrane (11). However, NEURON simulations of the standard cable model using three-dimensional morphologies of cortical pyramidal neurons give frequency scaling with an exponent $\alpha > 3$ (Fig. 1, C and D), suggesting that this is not a satisfactory explanation either.

None of the previous models take into account the fact that the surface of neuronal membranes is a complex arrangement, not only of phospholipids, but also of a wide diversity of surface molecules (12). This complex surface may be responsible for additional resistive phenomena not taken into account in previous approaches. In other words, the neuronal membrane may not be an ''ideal'' capacitor, as commonly assumed in the standard cable formalism. In this article, we explore this hypothesis as an alternative mechanism to explain the observed frequency scaling and consider neuronal membranes as ''nonideal'' capacitors. We show that cable equations can be extended by including a nonideal resistive component (Maxwell-Wagner time) in the capacitor representing the membrane, and that the nonideal cable model reproduces the observed frequency scaling. We also show consequences of this extension to cable equations in voltage attenuation and synaptic summation. Our aim is to provide an extended cable formalism which is more adapted to capture membrane potential dynamics and dendritic filtering at high frequencies. Some of these results have appeared in a conference abstract (13).

MATERIALS AND METHODS

The standard and nonideal cable equations were either solved analytically (see Results) or simulated using custom-made programs written in MatLab
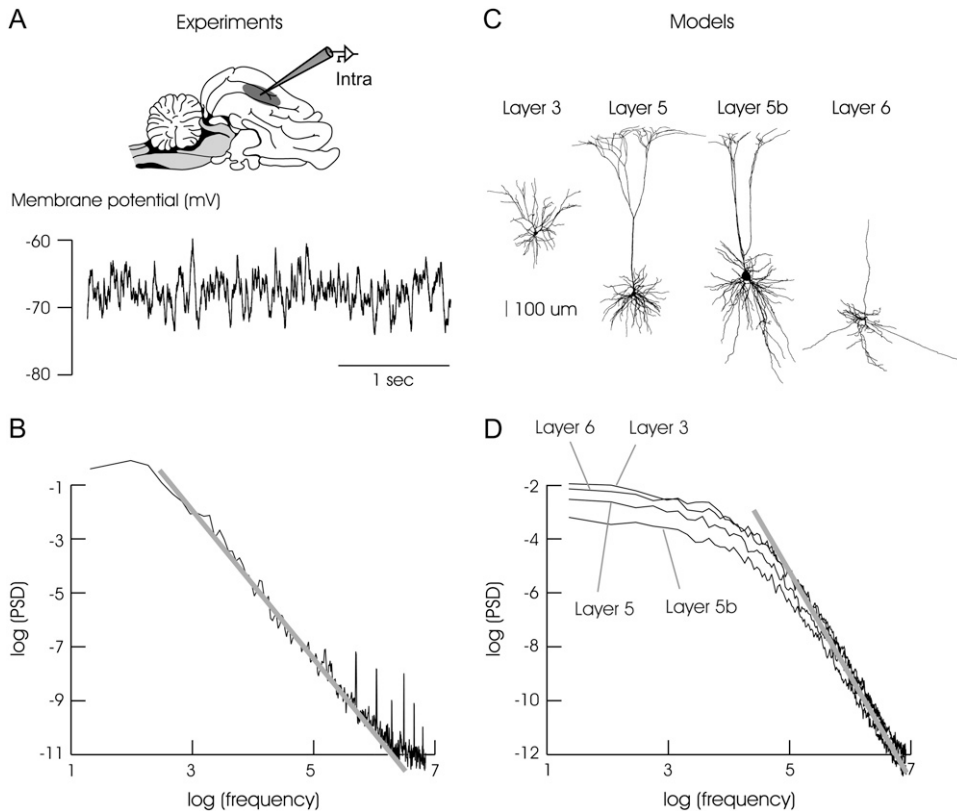
FIGURE 1 Fall-off structure of power spectra of synaptic noise in cortical neurons. (*A*) Time course of the membrane potential during electrically induced active states in a cortical neuron recorded intracellularly from cat parietal cortex in vivo (data from (7)). (*B*) Power spectral density (PSD) of the membrane potential in log scale. The PSD has a fall-off structure which follows a power law with a fractional exponent, at ~ -2.6 in this case (*dashed line*; modified from (4,7)). (*C*) Four different morphologies of cortical pyramidal neurons from cats obtained from previous studies (14,15), and which were incorporated into numerical simulations. (*D*) PSD obtained from the four models in panel *C*, using the traditional cable formalism in NEURON simulations. The power-law exponent obtained was of 3.4, 3.3, 3.2, and 3.4, respectively (cells shown from *left* to *right* in *C*).

(The MathWorks, Natick, MA). A ball-and-stick model consisting of a soma connected to a dendritic cylinder of length l_d was simulated (see Results for details). Away from the current source, we have the following equations (in Fourier space):

$$\lambda^2 \frac{\partial^2 V_m(x, \omega)}{\partial x^2} = \kappa_{ext}^2(\omega) V_m(x, \omega)$$

$$\kappa_{ext}^2(\omega) = 1 + i \frac{\omega \tau_m}{1 + i \omega \tau_M}, \qquad (1)$$

where $\lambda = \sqrt{r_m/r_i}$ is the electrotonic constant that characterizes the cable, τ_m is the membrane time constant, and τ_M is the Maxwell-Wagner time constant ($\tau_M = 0$ corresponds to the standard cable equations; see Results).

The source synaptic current consisted of a random synaptic bombardment of Poisson-distributed synaptic events. Each synaptic event consisted of an instantaneously rising current followed by exponential decay, and were summated linearly,

$$I_S = A \sum_i H(t - t_i) \exp[-(t - t_i)/\tau_S], \qquad (2)$$

where I_S stands for the source current, $H(t)$ is the Heaviside function, and t_i are the times of each synaptic event (Poisson-distributed with mean rate of 100 Hz). The decay time constant was $\tau_S = 10$ ms and the amplitude of the current was $A = 1$ nA.

The source current was inserted at different positions l_s in the dendrite (see Results). The voltage at the soma was obtained by solving either standard or nonideal versions of cable equations (see Results and Appendix 2). The power spectral density (PSD) was calculated from the somatic membrane potential using the fast Fourier transform algorithms present in MatLab (Signal Analysis toolbox). The same algorithm was also used to calculate the PSD from experimental data.

The experimental PSD of V_m activity shown here were obtained from intracellular recordings of cat parietal cortex neurons in vivo and were taken from previous publications (4,7), where all methodological details were given. No filter was used during digitization of the data, except for a low-pass filter with 5 kHz cutoff frequency during acquisition (sampling frequency of 10 kHz). Thus, the PSD is expected to reflect the real power spectral content of recorded V_m up to frequencies of 4–5 kHz.

Some simulations (Fig. 1, *C* and *D*) were realized using morphologically reconstructed neurons from cat cortex obtained from two previous studies (14,15), where all biological details were given. The three-dimensional morphology of the reconstructed neurons was incorporated into the NEURON simulation environment, which enables the simulation of the traditional cable equations using a three-dimensional structure with a controlled level of spatial accuracy (16). Simulations of up to 3500 compartments were used. In vivo-like activity was simulated using a previously published model of synaptic bombardment at excitatory and inhibitory synapses (17) (see this article for details about the numerical simulations).

RESULTS

We start by deriving the nonideal cable model, then investigate its general properties by evaluating the PSD of somatic voltage, as well as voltage attenuation.

Derivation of nonideal cable equations

The membrane as a nonideal capacitor

In electrostatics, if an electric field is applied to a closed conductive surface, electric charges migrate until they reach equilibrium (when the field tangential to the surface is zero). In particular, the electric resistivity of the membrane imposes

a given velocity to charge movement, which dissipates calorific energy similar to a friction phenomenon. This calorific dissipation is usually neglected, which amounts to considering an instantaneous charge rearrangement after changes in electric field.

However, in reality, this calorific dissipation may have significant consequences, and this phenomenon is well known for capacitors (18). A nonideal capacitor dissipates calorific energy when the electric potential varies, and capacitors are usually conceived such as to minimize this phenomenon and realize the well-known ideal relation $i = C(dV/dt)$. A nonideal linear capacitor can be represented as an arrangement of resistances, inductance, and capacitance (see Fig. 2 A). A linear approximation is usually sufficient for most purposes. In particular, this approximation is valid when the effects of electrostriction are negligible (10,19). This is the case when the propagated signals are of small amplitude (millivolts), because $C(V) = C(0)(1 + aV^2)$, with typically $a = 0.02\ V^{-2}$ (19). In such cases, the membrane capacitance can be represented by a resistance and a capacitance in series (20) (see Fig. 2 B). The resistance represents here the loss of calorific energy associated with charge movement. In standard cable equations, such a resistance is not present (see Fig. 2 C).

Thus, we use a more realistic capacitor modeled by taking into account an additional resistance (R_{sc}), which accounts for the calorific loss and the consequent finite-velocity of charge rearrangement. This R-C circuit will be characterized by a relaxation time $\tau_M = R_{sc}C$, called ''Maxwell time'' or ''Maxwell-Wagner time'' (21,22). The Maxwell time corresponds to the characteristic displacement time of the charges in the capacitor. Thus, such a nonideal capacitor cannot be charged instantaneously; the resistance R_{sc} imposes a minimal charging time due to finite charge velocities.

This phenomenon of finite charge velocity is particularly relevant to biological membranes, which are capacitors in which charges are also subject to rearrangements. In the following, we attempt to include this contribution to membrane capacitors by including Maxwell-Wagner time to cable equations and determine its consequences.

Nonideal cable equations

We extend cable equations by including a finite charge velocity (or equivalently, a minimal charging time) to membrane capacitors. We start by Ohm's law, according to which the axial current i_i in a cylindrical cable can be written as

$$i_i = \sigma \vec{E} = -\frac{1}{r_i}\frac{\partial V_m}{\partial x}. \tag{3}$$

We also have, for the membrane current i_m,

$$i_m = -\frac{(i_i(x + \Delta x) - i_i(x))}{\Delta x} \approx -\frac{\partial i_i}{\partial x}, \tag{4}$$

and we can write

$$i_m = \frac{V_m}{r_m} + \int_{-\infty}^{\infty} \frac{\partial c_m(t - t')}{\partial t} V_c(t')dt', \tag{5}$$

where $c_m(t)$ is the inverse complex Fourier transform of the capacitance $c_m(\omega)$. Note that $c_m(t) = c_m\delta(t)$ if the capacitance does not depend on the frequency.

Integrating Maxwell-Wagner phenomena, we have

$$V_m = V_c + r_{sc} \int_{-\infty}^{\infty} \frac{\partial c_m(t - t')}{\partial t} V_c(t')dt'.$$

Thus, we obtain the following nonideal cable equations:

$$\lambda^2 \frac{\partial^2 V_m}{\partial x^2} = V_m + r_m \int_{-\infty}^{\infty} \frac{\partial c_m(t - t')}{\partial t} V_c(t')dt'$$

$$V_m = r_{sc} \int_{-\infty}^{\infty} \frac{\partial c_m(t - t')}{\partial t} V_c(t')dt' + V_c, \tag{6}$$

where $\lambda = \sqrt{r_m/r_i}$ is the electrotonic constant that characterizes the cable.

General solution of nonideal cable equations

The nonideal cable equations (the expressions in Eq. 6) are a linear system with constant coefficients which can be solved by using Complex Fourier Transforms:

$$v_m(x, \omega) = \int_{-\infty}^{\infty} V_m(x, t)\, e^{i\omega t}\, dt$$

$$v_c(x, \omega) = \int_{-\infty}^{\infty} V_c(x, t)\, e^{i\omega t}\, dt$$

$$c_m(\omega) = \int_{-\infty}^{\infty} c_m(t)\, e^{i\omega t}\, dt.$$

We obtain the expression

$$\lambda^2 \frac{d^2 v_m(x, \omega)}{dx^2} = \kappa_{ext}^2 v_m(x, \omega) \tag{7}$$
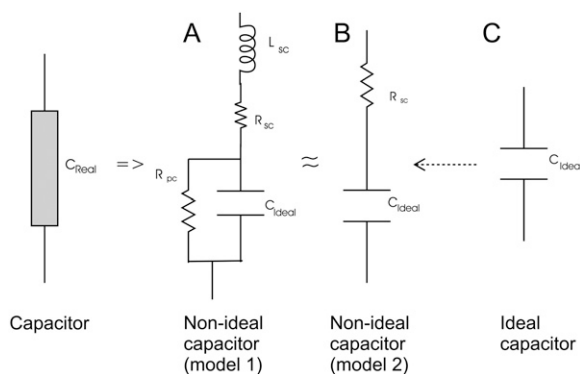

FIGURE 2 Different equivalent electric schemes for capacitors. (A) Linear model of a capacitor, consisting of two resistances (R_{sc} and R_{pc}), one inductance (L_{sc}), and one capacitance element (C). (B) Approximation of the linear model obtained by including a resistance (R_{sc}) in series with the capacitance (C). This leads to a characteristic relaxation time for charging the capacitor (given by $\tau_M = R_{sc}C$). (C) Ideal capacitance as in the standard cable model.

with

$$\kappa_{ext}^2 = 1 + i\frac{\omega\tau_m}{1 + i\omega\tau_M}, \qquad (8)$$

where $\tau_m(\omega) = r_m c_m(\omega)$ and $\tau_M(\omega) = r_{sc} c_m(\omega)$ are the parameters that characterize the cable.

The general solution of Eq. 7 is given by

$$v_m(x,\omega) = A(\omega)\exp\left(\frac{\kappa_{ext}(l_s - x)}{\lambda}\right)$$
$$+ B(\omega)\exp\left(-\frac{\kappa_{ext}(l_s - x)}{\lambda}\right), \qquad (9)$$

where l_s is the position of the current source in the dendrite.

This solution is similar to that of traditional cable equation, with the only difference in the value of κ. In cable equations, this value is given by

$$\kappa_s^2 = 1 + i\omega\tau_m. \qquad (10)$$

In particular, for null frequency, the two cable formalisms are equivalent

$$\kappa_{ext}(0) = \kappa_s(0) = 1, \qquad (11)$$

whereas they will predict different behavior for $\omega > 0$.

In the following, we will consider that the capacitance is independent of frequency, $c_m(\omega) = cst$, as also assumed in the standard cable model (1,2).

Fig. 3 compares the values of κ between the two cable formalisms (with $c_m(\omega) = cst$). The difference depends on the relative values of τ_M and τ_m: for $\tau_M \ll \tau_m$, the two formalisms are very similar, but differ when τ_M is larger, in particular for high frequencies. Thus, the critical parameter is τ_M, which determines the saturation of the value of κ.
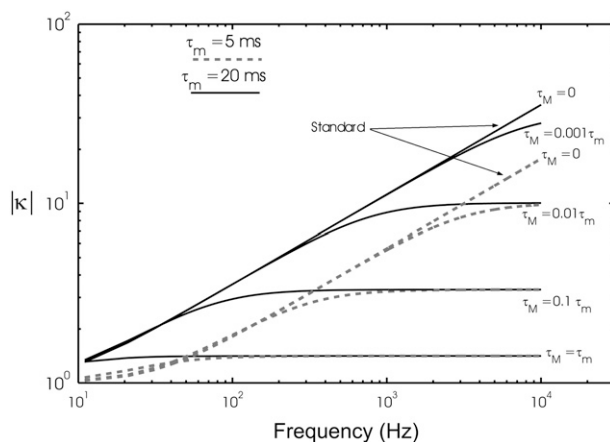

FIGURE 3 Comparison between κ-values in the standard and nonideal cable model. The values of κ are plotted for the two models for various values of τ_M and two values of τ_m (5 ms and 20 ms). The function κ saturates for the nonideal cable model, and the value of the saturation equals to $\sqrt{1 + \tau_m/\tau_M}$. The κ curves for the nonideal model depart from the standard model for a frequency that approaches the cutoff frequency of $f_c = 1/(1/2\pi\tau_M)$.

Voltage attenuation versus distance and frequency

To compare the properties of the nonideal cable model compared to the standard cable model, we evaluated the properties of voltage attenuation in a large dendritic branch. We have chosen a cable of $l_d = 500$ μm and diameter of 2 μm, with a current source situated at one end of the cable ($x = l_s = 0$) and connected to an infinite impedance at the other end ($x = l_d$; sealed end). In these conditions, we can determine the law of voltage attenuation with distance, using complex Fourier analysis.

As we have seen above, the main difference between the standard and nonideal cable models lies in the expression for κ (see Eqs. 8 and 10). In a finite cable of constant diameter, the steady-state voltage attenuation profile is given by the relation

$$V_m(x,\omega) = A(\omega)\exp\left(-\frac{\kappa}{\lambda}x\right) + B(\omega)\exp\left(\frac{\kappa}{\lambda}x\right), \qquad (12)$$

for $x > 0$. To evaluate the functions $A(\omega)$ and $B(\omega)$, we apply the limit conditions of the dendrite. At $x = 0$, we have a current source $i_s = 1 = i_d$, and at $x = l_d$ we have $i_d = 0$ (sealed end). The expressions for A and B are then given by Eqs. 19 and 20, respectively (see Appendix 2).

This relation is plotted in Fig. 4 for two values of the membrane time constant τ_m of 5 ms and 20 ms, which correspond to two different conductance states of the membrane (the corresponding electrotonic constant is $\lambda = 353.5$ μm and 707.1 μm, respectively). The voltage attenuation is in general steeper for the nonideal cable model, which effect is particularly apparent for frequencies of the order of 0–50 Hz. However, this effect reverses between 50 and 100 Hz, in which case the nonideal cable model shows a less steep voltage attenuation profile compared to the standard cable model (see 50 and 100 Hz in Fig. 4).

Power spectra of voltage noise predicted by nonideal cable equations

We now calculate the PSD of the voltage noise predicted by nonideal cable equations. We consider a ball-and-stick model consisting of a soma and a dendritic segment of variable length (Fig. 5 A). The source consists of a sum of exponentially decaying currents (see Materials and Methods), which represent the synaptic current resulting from many synapses releasing randomly, as shown in Fig. 5 B. The source has a PSD which scales as $1/f^\alpha$ with an exponent $\alpha = 2$ at high frequencies (Fig. 5 C).

To investigate the PSD of the somatic voltage in the ball-and-stick model, we first examine the PSD after a single source consisting of summated exponential synaptic currents. The standard cable model predicts that such a source localized on a dendritic branch (ball-and-stick model with $l_d = 500$ μm and $\lambda \simeq 400$ μm) gives a V_m PSD scaling
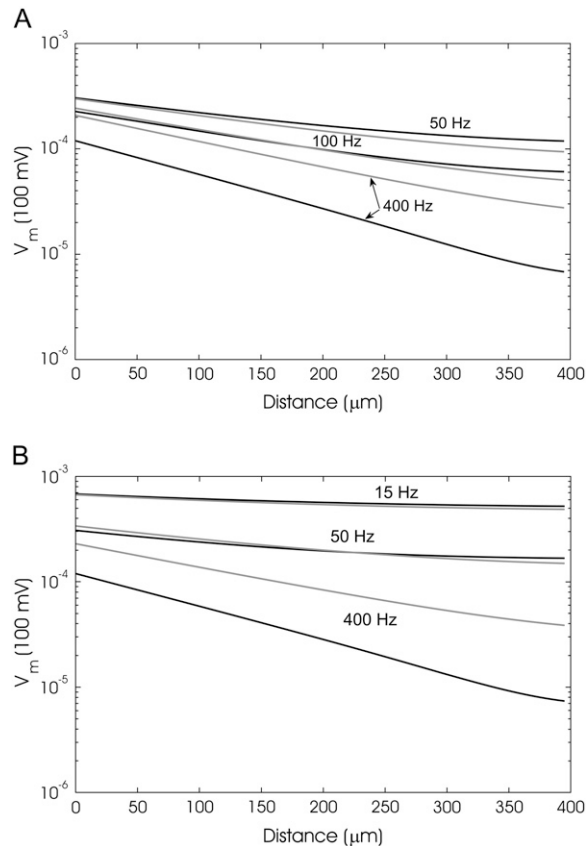
FIGURE 4 Steady-state voltage profile in a finite cable. A cable of 500-μm length and 2-μm diameter was considered with a current source at $x = 0$ ($C_m = 1$ μF/cm^2; $R_i = 2$ Ωm). The voltage profiles in the nonideal (*shaded lines*) and standard (*solid lines*) cable models are compared for different frequencies. Two values of the membrane time constant are considered, (*A*) $\tau_m = 5$ ms and (*B*) $\tau_m = 20$ ms, which correspond to two different conductance states ($\tau_M = 1.5$ ms in both cases, which corresponds to $\tau_M = 0.3$ τ_m in A, and $\tau_M = 0.075$ τ_m in B).

FIGURE 5 Ball-and-stick model used for calculations. (*A*) Scheme of the ball-and-stick model where P indicates the soma, S the position of the current source, and $Z_1 \ldots Z_3$ are impedances used in the calculation. (*B*) Example of a source current representing synaptic bombardment in the ball-and-stick model. The current source consists of Poisson-distributed exponential currents (see Materials and Methods). (*C*) Power spectral density of the synaptic current source shown in panel B. The PSD scales as a Lorentzian ($1/f^\alpha$ with an exponent $\alpha = 2$ between 100 and 400 Hz).

approximately as $1/f^\alpha$ with an exponent $\alpha \simeq 4$, which corresponds to a somatic impedance much larger than that of the dendrite (soma radius of 7.5 μm; see Appendix 1), which would correspond to most central neurons for which the soma represents a minor proportion of the membrane. The V_m PSD for the standard cable model with uniformly distributed exponential synaptic currents is illustrated in Fig. 6 (*continuous curve*), and shows a frequency scaling with an exponent $\alpha \simeq 4$.

In contrast, the nonideal cable model gives different scaling properties of the PSD, according to the value of τ_M (Fig. 6, *dotted* and *dashed lines*). The power for high frequencies (>50 Hz) is much larger in the nonideal cable model compared to the standard model, which shows that nonideal cables have enhanced signal propagation for high frequencies. The V_m PSD for the nonideal cable model with uniformly distributed exponential synaptic currents is illustrated in Fig. 6 (*dashed curve*), and shows a frequency scaling with an exponent $2 < \alpha \leq 4$ for $\tau_m \geq \tau_M \geq 0$,
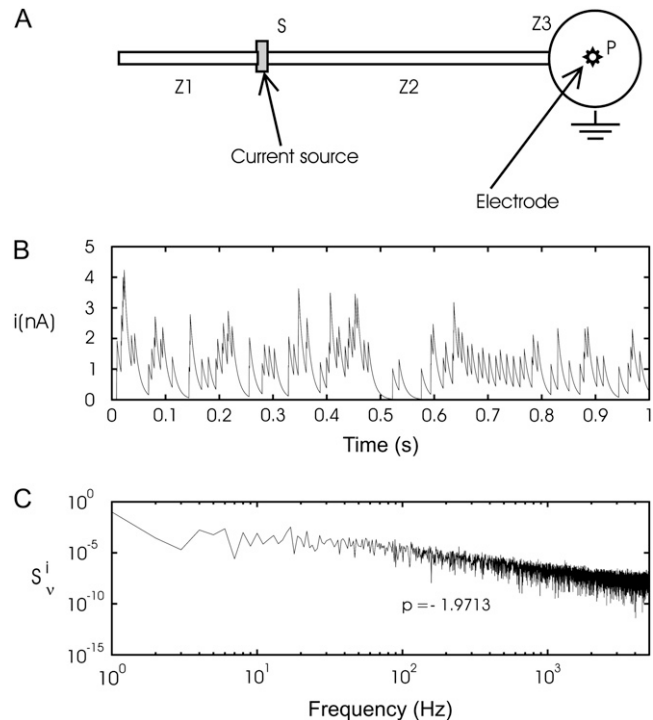
respectively ($\alpha \simeq 2$ when $\tau_m = \tau_M$, but it can be shown that $\alpha = 2$ only if $\tau_M \to \infty$).

We next investigated the influence of the localization of the current source in the dendrite. Fig. 7 *A* shows the PSD obtained at the soma of the ball-and-stick model when the current source was placed at different positions in the dendrite. The position affects the amplitude of the PSD, and the frequency-scaling of the PSD is affected by the position. The scaling exponents obtained are of $\alpha = 4.1416$ for 250 μm and 5.3653 for 450 μm for the standard model, and $\alpha = 2.5311$ for 250 μm and 2.8354 for 450 μm for the nonideal cable model. The PSD obtained when simulating a distributed synaptic bombardment in the dendrite (Fig. 7 *B*) also displays the same frequency-scaling. Similar results were also obtained by varying the parameters τ_m and τ_M (not shown), suggesting that the properties of frequency scaling, as shown in Fig. 6, are generic.

To evaluate the optimal value of τ_M (for this particular model with $\tau_m = 5$ ms), we fitted the PSD of the model to that of experiments. To perform this fit, we used a frequency range of 100 to 400 Hz, which was chosen such that it is not affected by instrumental noise (<700 Hz) and such that the frequency band considered belongs to the power-law scaling
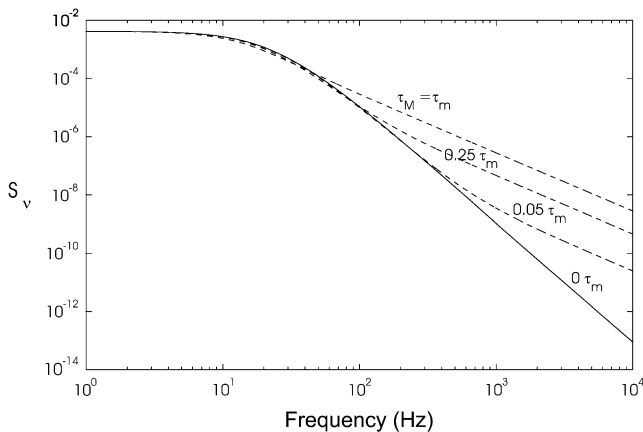
FIGURE 6 Power spectral density of the V_m of the ball-and-stick model with exponential synaptic currents uniformly distributed in the dendrite (from 1 to 450 μm, every 10 μm). The current source of each synaptic event was the same and equals $\exp(-t/0.1)$ nA, and the PSD is shown for the membrane potential at the soma. The continuous curve shows the standard cable model, while the other curves (*dotted* and *dashed*) show the nonideal cable model with different values of τ_M. Parameter values: $C_m = 1\ \mu$F/cm^2, $\tau_m = 5$ ms, $l_d = 500\ \mu$m, $R_d = 1\ \mu$m, $R_{soma} = 7.5\ \mu$m, and $R_i = 2\ \Omega$m.

region of the spectra (> 80 Hz). The result of this fitting is shown in Fig. 8. The scaling exponents obtained are of $\alpha = 3.6533$ for the standard cable model, and of $\alpha = 2.3306$ for the nonideal cable model, for an optimal value of $\tau_M = 0.3\ \tau_m$. This suggests that the calorific dissipation caused by the resistivity of the membrane to charge movement is $\sim$30% of that caused by the flow of ions through ion channels. This estimate is of course specific to the model used, but variations of this model (l_d, diameter, number of dendrites, for a uniform τ_m over the whole neuronal surface) showed little variation around this value (not shown).

This value gives a cutoff frequency ($1/\tau_M$) at $\sim$105 Hz. Above this cutoff frequency, the membrane becomes more resistive than capacitive because the energy loss due to calorific dissipation becomes larger than the energy necessary for charge displacement. This is very different from an ideal capacitor, in which the energy from the current source would exclusively serve to charge displacement. In Fig. 3, one can see that the value of κ for the nonideal model departs from that of the standard cable model around this cutoff frequency.

Thus, from the above figures, and especially Fig. 6, it is apparent that the nonideal cable model has more transmitted power compared to the standard cable model at high frequencies ($\gg$100 Hz). This increased transmission of high frequencies is also visible by superimposing the V_m activities of the standard and nonideal model (Fig. 9). Such an increased transmission at high frequencies can be explained by the fact that in the standard cable model, the term $1/i\omega c_m$ tends to zero when ω tends to infinity, such that, for high frequencies, r_m is short-circuited by the capacitance of the membrane. In the nonideal cable model, such a short-circuit
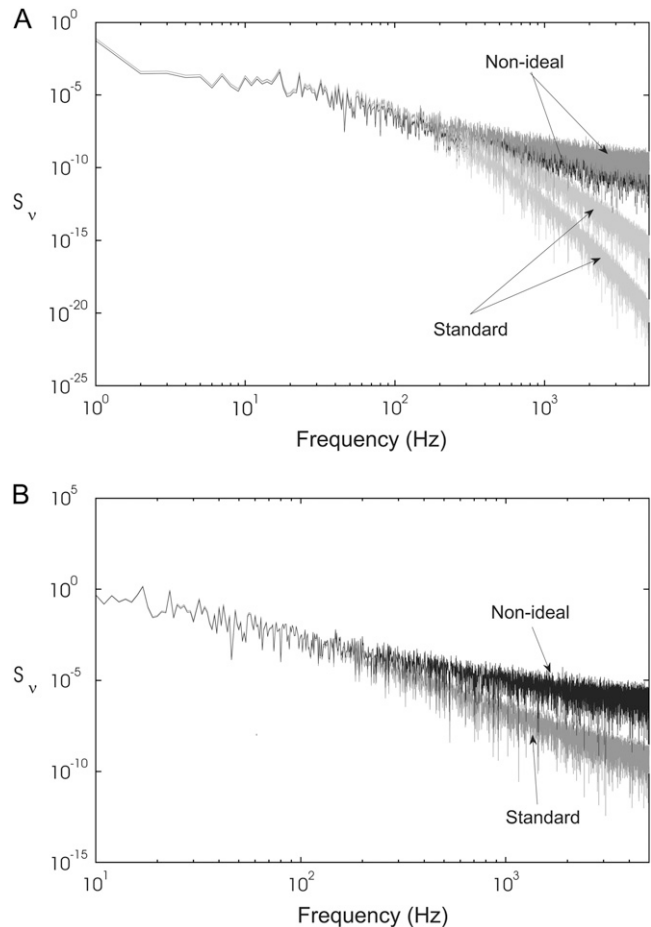

FIGURE 7 Power spectral density of multiple synaptic events in the ball-and-stick model. (*A*) Voltage PSD at the some for a source current similar to Fig. 5 *B* which was placed at different positions in the dendrite (from *top* to *bottom*: 250 and 450 μm from the soma). For each location, the PSD is shown for the standard cable model (*shaded*) and for the nonideal cable model (*solid*). (*B*) PSD obtained when the source currents were distributed in the dendrite (from 1 to 450 μm, every 10 μm). Parameter values: $C_m = 1\ \mu$F/cm^2, $\tau_m = 5$ ms, $l_d = 500\ \mu$m, $R_d = 1\ \mu$m, $R_{soma} = 7.5\ \mu$m, $R_i = 2\ \Omega$m, and $\tau_M = 0.3\ \tau_m$.

does not occur, even at frequencies much larger than the cutoff frequency. This results in a very different behavior at high frequencies, and a less pronounced frequency falloff in the nonideal cable PSD. Displacing charges by capacitive effect takes energy, and this energy diminishes with increasing frequencies in the nonideal cable, which enables more energy transfer between remote ion channels in dendrites (synapses, for example) and the soma at high frequencies. This is also consistent with the fact that the nonideal cable equations display less voltage attenuation (see Voltage Attenuation Versus Distance and Frequency).

DISCUSSION

In this article, we have proposed an extension to the classic cable theory to account for the behavior of neuronal
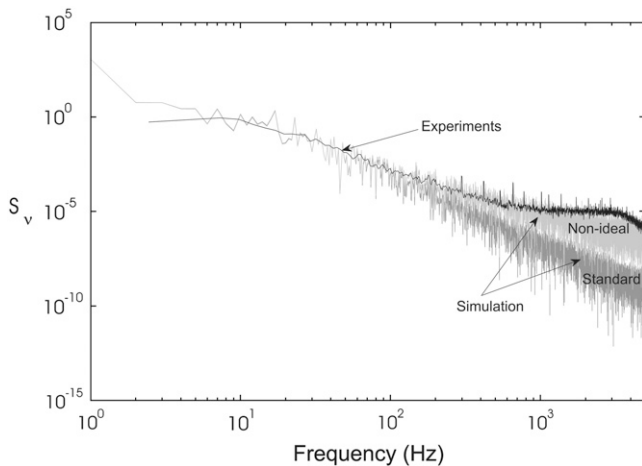
FIGURE 8 Best fit of the nonideal cable model to the power spectral density obtained from intracellular experiments. The nonideal cable model was simulated using a ball-and-stick model subject to synaptic bombardment (see Materials and Methods). The dendritic branch had a 75-μm length and the power spectral density (PSD) was calculated from the somatic membrane potential. (*Solid*) Experimental PSD (see Fig. 1); (*shaded*) model PSD (see Fig. 5 *C* for the PSD of the current source). The slopes were calculated using a linear regression in the frequency band 100–400 Hz. The optimal value for τ_M was of 0.3 τ_m. Parameter values: $C_m = 1$ μF/cm^2, $\tau_m = 5$ ms, $l_d = 75$ μm, $R_d = 1$ μm, $R_{soma} = 7.5$ μm, and $R_i = 2$ Ωm.

membranes at high frequencies. Experimental observations indicate that the PSD of the V_m does not match that predicted from cable theory, in particular for the frequency-scaling at high frequencies (4–7). The modification to cable equations consists of incorporating a nonideal membrane capacitance by taking into account the calorific dissipation due to charge displacement, which is usually neglected. We have shown that this nonideal cable formalism can account for the frequency scaling of the PSD observed experimentally for high frequencies (Fig. 8).

In experiments with channel noise or synaptic noise, the V_m PSD scales as $1/f^\alpha$ with an exponent α at $\sim$2.5 (4–7). The standard cable model predicts that the somatic V_m should scale with an exponent α comprised between 3 and 4 (5),
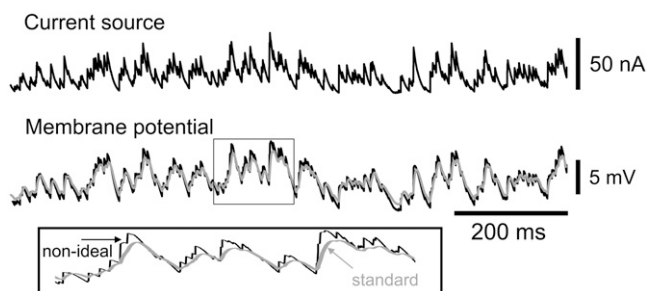

FIGURE 9 Comparison of V_m activities in the standard and nonideal cable models. The current source is indicated on top, while the bottom trace shows the V_m activities superimposed. The inset shows a detail at five-times higher temporal resolution. Same parameters as the optimal fit in Fig. 8.

when the source is located in the soma. However, we have shown here that the frequency scaling of the V_m PSD depends on the location of the source, and that the exponent α is equal or larger when current sources are located in dendrites (see Fig. 7 and Appendix 1). Thus, the standard cable model cannot account for exponents lower than $\alpha = 3$. On the other hand, taking into account nonideal capacitances may lead to scaling exponents down to $\alpha = 2$, depending on the magnitude of the dissipation in the nonideal capacitance (as quantified by the value of the Maxwell-Wagner time τ_M; see Fig. 6). In the case that τ_M is nonuniform, one may then have larger differences of frequency scaling between somatic and dendritic current sources (not shown).

In the nonideal model, the calorific dissipation originates mostly from the resistance of the membrane to lateral ion displacement. This tangential resistance is not yet characterized experimentally and is equivalent to the resistance involved in the noninstantaneous character of membrane polarization (22). Several arguments indicate that this resistance may be substantial. First, the membrane surface contains various molecules such as sugars and various macromolecules, in addition to phospholipids (12). Thus, lateral ion movement is likely to be affected by collisions or tortuosity imposed by these molecules. Second, the phospholipids themselves contain local dipoles at their polar end, which is likely to cause local electrostatic interactions which may influence the lateral movement of ions. Indeed, the fitting to experimental data using the nonideal cable model predicts a value for τ_M, which is a significant fraction ($\sim$30%) of the membrane time constant.

The complex three-dimensional membrane morphology could have consequences on frequency-dependent properties even with traditional cable theory (11). We tested this possibility by simulating detailed three-dimensional morphological models of cortical pyramidal neurons and failed to reproduce the frequency scaling of the V_m activity in vivo (see Fig. 1). Thus, although the morphology does affect frequency scaling, it does not account for the values observed experimentally.

Another source of distortion in the frequency dependence of the V_m is the fact that membrane permittivity (and capacitance) may also depend on frequency (9,23). Such a frequency dependence is caused by a calorific dissipation during the polarization of the membrane (9), while the Maxwell-Wagner phenomenon that we discuss here is a calorific dissipation during the movement of charges on the membrane surface. However, direct capacitance measurements of bilipid membranes do not evidence any significant variation of permittivity for frequencies at $\sim$100 Hz (10), and thus cannot explain the observed deviations between cable theory and experiments shown in Fig. 1. Moreover, these measurements (10,19) were realized on artificially reconstructed membranes, which have a much simpler structure compared to neuronal membranes (no saccharides, no proteins, etc.). This is compatible with the possibility that in biological membranes, the Maxwell-Wagner effect may be particularly

prominent. The dependence of the membrane capacitance c_m on frequency may explain the flattening of the PSD above 1000 Hz, which is visible in the experimental PSDs (see Fig. 8). However, the most likely explanation for this flattening is that the recording is dominated by instrumental noise at such frequencies (note that the bending of the experimental PSD above 4000 Hz in Fig. 8 is likely due to the low-pass 5 kHz filter used during data acquisition).

Other factors may also affect the frequency scaling. Taking into account the finite rise time of synaptic events by using double-exponential templates amounts to add a factor 2 to the exponent α (8). Similarly, introducing correlations in the presynaptic activity may also affect the frequency scaling of V_m power spectra (24). In all these cases, however, the change in the scaling always consists of increasing the exponent α, while a decrease is needed to account for $\alpha = 2.5$ scaling.

Thus, the frequency scaling of the V_m activity can be affected by several factors as discussed above. Our results show that the nonideal character of the neuronal membrane can account for the observed frequency scaling. We believe that, in reality, a combination of factors is responsible for the observed frequency scaling, and future experiments should be designed to test which are the most determinant on frequency scaling, and what are the consequences on the integrative properties of neuronal cable structures.

Finally, our results show that the frequency-dependence of the steady-state voltage profile (Fig. 4) is also affected by the nonideal character of the membrane capacitance. Simulations show that high-frequency signals (>100 Hz) propagate over larger distances in the nonideal cable model compared to the standard cable model. This theoretical result may be important to understand the propagation of high-frequency events such as the ''ripples'' oscillations (25,26) across dendritic structures.

In conclusion, we provided here an extension to cable equations which incorporates the nonideal character of the membrane capacitance. We showed that this extension yields several detectable consequences on neurons. First, it affects basic cable properties such as the voltage attenuation profile, especially at high frequencies. Second, it radically changes the frequency-scaling properties of voltage power spectra. The observed frequency scaling is within the range predicted by the nonideal cable model. Fitting the model to experiments provides an estimate of how nonideal is the membrane capacitance, and the significant values of τ_M found here suggest that, indeed, neuronal membranes may be far from being ideal capacitors.

APPENDIX 1: FREQUENCY SCALING IN THE STANDARD CABLE MODEL

In this Appendix, we overview the frequency scaling characteristics of the PSD of the V_m for the ball-and-stick model using the standard cable equations.

Dendritic current source located close to the soma

We first consider the ball-and-stick model with an isolated current source located in the dendrite close to the soma. From Eq. 24 (see Appendix 2), we have

$$(Z_2 \oplus Z_3)_{l \approx 0} \approx \lim_{l \to 0}(Z_2 \oplus Z_3) = Z_3,$$

and from Eq. 21, when the distance l from the source to the soma is small, the impedance of the distal part of the dendrite is given by

$$Z_1 \approx \frac{\lambda r_i}{\kappa_s} \coth\left(\frac{\kappa_s l_d}{\lambda}\right),$$

where l_d is the length of the dendrite. From Eq. 14, for small l, we have

$$V_E = F_A i_S \approx \left(\frac{\lambda r_i}{\kappa_s} \| Z_3\right) i_S,$$

where $\lambda r_i / \kappa_s$ is the input impedance of a finite dendritic branch. Thus, from Eq. 28, for small l, we obtain

$$F_T(l, \omega) \approx \lim_{l \to 0} F_T(l, \omega) = 1.$$

Because $F_B \simeq 1$, the membrane potential at the center of the soma is given by

$$V_{soma} = \left(\frac{\lambda r_i}{\kappa_s} \| Z_3\right) i_S, \tag{13}$$

when the current source is located close to the soma.

Thus, for high frequencies (>100 Hz), the PSD of the somatic V_m scales as $1/f^\alpha$ with $\alpha \in (3,4)$ for a exponential current source located close to the soma. This result is similar to single-compartment models (8).

General case of dendritic current source

We now consider the general case of a current source located at an arbitrary position in the dendritic branch of the ball-and-stick model. We have necessarily $F_T \neq 1$, resulting in a supplementary dependence on frequency. Moreover, the current divider F_A also depends on frequency. Numerical simulations show that the PSD of the somatic V_m scales as $1/f^\alpha$ with an exponent $\alpha > 3$. For example, with exponential currents uniformly distributed on a dendrite of $l_d = 500$ μm, the frequency scaling is close to an exponent of $\alpha = 4$ (see *continuous curve* in Fig. 6). We verified numerically (not shown) that the standard cable model cannot give a frequency scaling with a slope smaller than $\alpha = 3$ (using Poisson-distributed synaptic inputs).

A similar scaling with an exponent $\alpha = 4$ was observed earlier, when simulating realistic dendritic morphologies based on reconstructed cortical pyramidal neurons (8).

APPENDIX 2: IMPEDANCE ANALYSIS OF THE BALL-AND-STICK MODEL

In this Appendix, we derive the expressions needed to study the frequency dependence of the ball-and-stick model (Fig. 5 *A*), for both standard and nonideal cable equations. The ball-and-stick model consists of a soma, which is assumed to be the recording site, and a dendritic branch which contains the source. Referring to Fig. 5 *A*, we have the source (S) and the recording locations (P), as well as the impedances corresponding to the different regions (Z_1 for the distal part of the dendrite, away of the source, Z_2 for the proximal part of the dendrite, between the source and the soma, and Z_3 for the soma).

We first evaluate the voltage at the current source:

$$V_s = i_s \frac{Z_1 (Z_2 \oplus Z_3)}{Z_1 + (Z_2 \oplus Z_3)} = F_A i_s, \qquad (14)$$

where the term $(Z_2 \oplus Z_3)$ is the input impedance of the dendritic segment in series with Z_3. F_A is the input impedance as seen by the current source i_s located at a position l_s on the dendritic branch. Equation 14 shows how F_A varies as a function of the position of the source in the dendrite.

Next, we calculate the somatic voltage from the transfer function of the dendritic branch, F_T, which links the voltage at the source with the somatic voltage,

$$V_{soma} = F_T V_E. \qquad (15)$$

Finally, we calculate the voltage transferred to the soma from the equivalent circuit (Fig. 10),

$$V_P = \frac{Z_{3b}}{Z_{3a} + Z_{3b}} V_{soma} = F_B V_{soma}, \qquad (16)$$

where F_B is the voltage divider caused by the fact that the tip of the recording pipette is located inside the soma at some distance from the membrane (in case of sharp-electrode recordings). This divider is entirely resistive and very close to 1, which expresses the fact that the exact position of the pipette is not a determining factor in the value of V_P.

Thus, we have

$$V_{soma} = F_B F_T F_A i_s \simeq F_T F_A i_s. \qquad (17)$$

We calculate these different terms below.

Input impedance Z_1 (distal part of the dendrite)

For a current source i_s located at position l_s, we have

$$i_s = i_{d_1}(l_s, \omega) + i_{d_2}(l_s, \omega), \qquad (18)$$

where $i_{d_1}(l_s, \omega)$ is the current density at the beginning of the distal part of the dendrite (of length Δl_1), and $i_{d_2}(l_s, \omega)$ is the current density of the proximal part of the dendrite (see Fig. 10). From Eq. 9, we have

$$i_{d_1}(l_s, \omega) = -\frac{1}{r_i} \frac{\partial v_m(l_s + |\varepsilon|, \omega)}{\partial x} = \frac{\kappa}{\lambda r_i}(B - A),$$

where $|\varepsilon| > 0$ can be as small as desired. This factor arises because we consider point current sources, in which case the spatial derivative of the V_m is discontinuous at $x = l_s$.
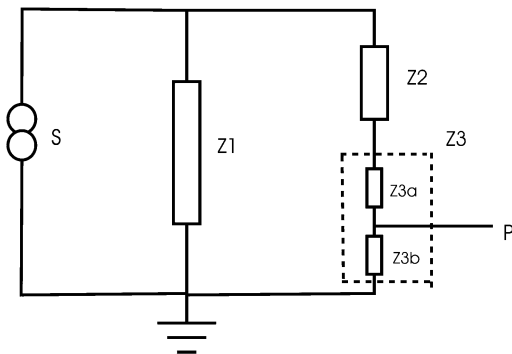

FIGURE 10   Equivalent circuit for the ball-and-stick model. Z_1 is the input impedance of the dendritic branch (*open circuit*), and Z_2 is the impedance of the intermediate segment, in series with the impedance Z_3 of the soma.

From the ''sealed end'' condition, we have

$$i_{d_1}(l_s + \Delta l_1, \omega) = -\frac{1}{r_i} \frac{\partial v_m}{\partial x}(l_s + \Delta l_1, \omega)$$

$$= -\frac{\kappa}{\lambda r_i} \left[A(\omega) \exp\left(-\frac{\kappa \Delta l_1}{\lambda}\right) \right.$$

$$\left. - B(\omega) \exp\left(\frac{\kappa \Delta l_1}{\lambda}\right) \right] = 0.$$

Thus, we have

$$A(\omega) = \frac{\lambda r_i}{\kappa} \frac{\exp\left(\dfrac{2\kappa \Delta l_1}{\lambda}\right)}{1 - \exp\left(\dfrac{2\kappa \Delta l_1}{\lambda}\right)} \qquad (19)$$

and

$$B(\omega) = \frac{\lambda r_i}{\kappa} \frac{1}{1 - \exp\left(\dfrac{2\kappa \Delta l_1}{\lambda}\right)}. \qquad (20)$$

Consequently, we obtain

$$Z_1 = \frac{v_m(l_s, \omega)}{i_{d_1}(l_s, \omega)} = \frac{\lambda r_i}{\kappa} \coth\left(\frac{\kappa \Delta l_1}{\lambda}\right), \qquad (21)$$

where $\kappa = \kappa_s$ or κ_{ext} for standard or nonideal cable models.

Input impedance $(Z_2 \oplus Z_3)$ (proximal region)

For the proximal part of the dendrite (of length $\Delta l_2 = l_s$), which is in series with the impedance Z_3 at $x = 0$ (see Fig. 10), we have (see Eqs. 18 and 9)

$$i_{d_2}(l_s, \omega) = -\frac{1}{r_i} \frac{\partial v_m(l_s - |\varepsilon|, \omega)}{\partial x} = \frac{\kappa}{\lambda r_i}(B - A),$$

where $|\varepsilon| > 0$ can be as small as desired.

Moreover, we have

$$i_{d_2}(0, \omega) = -\frac{1}{r_i} \frac{\partial v_m}{\partial x}(0, \omega) = -\frac{\kappa}{\lambda r_i} \left[A(\omega) \exp\left(\frac{\kappa l_s}{\lambda}\right) \right.$$

$$\left. - B(\omega) \exp\left(-\frac{\kappa l_s}{\lambda}\right) \right] = \frac{v_m(0, \omega)}{Z_3}$$

and

$$v_m(0, \omega) = A(\omega) \exp\left(\frac{\kappa l_s}{\lambda}\right) + B(\omega) \exp\left(-\frac{\kappa l_s}{\lambda}\right).$$

Thus, we obtain

$$B(\omega) = A(\omega) \frac{\left(1 + \dfrac{\lambda r_i}{\kappa Z_3}\right)}{\left(1 - \dfrac{\lambda r_i}{\kappa Z_3}\right)} \exp\left(\frac{2\kappa l_s}{\lambda}\right)$$

and

$$B(\omega) = A(\omega) + \frac{\lambda r_i}{\kappa} i_{d_2}(l_s, \omega).$$

Consequently, we obtain

$$A(\omega) = \frac{\lambda r_i \left[\kappa Z_3 - \lambda r_i\right] i_{d_2}(l_s, \omega)}{\kappa \left[\exp\left(\dfrac{2\kappa l_s}{\lambda}\right) + 1\right]\left[\kappa Z_3 \tanh\left(\dfrac{\kappa l_s}{\lambda}\right) + \lambda r_i\right]} \quad (22)$$

and

$$B(\omega) = \frac{\lambda r_i \left[\kappa Z_3 + \lambda r_i\right] i_{d_2}(l_s, \omega) \exp\left(\dfrac{2\kappa l_s}{\lambda}\right)}{\kappa \left[\exp\left(\dfrac{2\kappa l_s}{\lambda}\right) + 1\right]\left[\kappa Z_3 \tanh\left(\dfrac{\kappa l_s}{\lambda}\right) + \lambda r_i\right]}. \quad (23)$$

Thus, the input impedance $(Z_2 \oplus Z_3)$ is given by

$$(Z_2 \oplus Z_3) = \frac{v_m(l_s, \omega)}{i_{d_2}(l_s, \omega)} = \frac{\lambda r_i \cdot Z_3}{\left[\kappa Z_3 \tanh\left(\dfrac{\kappa l_s}{\lambda}\right) + \lambda r_i\right]}$$
$$+ \frac{\lambda^2 r_i^2 \tanh\left(\dfrac{\kappa l_s}{\lambda}\right)}{\kappa \left[\kappa Z_3 \tanh\left(\dfrac{\kappa l_s}{\lambda}\right) + \lambda r_i\right]}, \quad (24)$$

where $\lambda = \sqrt{r_m/r_i}$ and $\kappa = \kappa_s$ or κ_{ext} according to which cable model is used.

For $Z_3 \rightarrow \infty$, we obtain the input impedance from Eq. 21.

Calculation of the transfer function F_T

To evaluate F_T, we calculate the voltage at point $x = l$ by imposing $v_m(l_s, \omega) = 1$ at point $x = l_s$. With this initial value, the voltage $v_m(x)$ at point $x = 0$ equals the value of the transfer function at point $x = 0$ (see Eq. 9). In such conditions, we obtain

$$A(\omega) + B(\omega) = 1.$$

Thus, we have

$$F_T(x, \omega) = A(\omega)\left[\exp\left(\frac{\kappa}{\lambda}(l_s - x)\right) - \exp\left(-\frac{\kappa}{\lambda}(l_s - x)\right)\right]$$
$$+ \exp\left(-\frac{\kappa}{\lambda}(l_s - x)\right). \quad (25)$$

The voltage v_m at point $x = 0$ must equal $Z_3 i_i(l, \omega)$ (current conservation). We have

$$\frac{\partial v_m}{\partial x} = -r_i i_i.$$

Consequently, we must obtain

$$\left.\frac{\partial F_T}{\partial x}\right|_{x=0} = -r_i \frac{v_m}{Z_3}\bigg|_{x=0} = \eta\, v_m\,|_{x=0} = \eta\, F_T|_{x=0}, \quad (26)$$

where $\eta = -r_i/Z_3$. Thus, we have

$$A(\omega) = \frac{(\kappa - \lambda\eta)\exp\left(-\frac{\kappa l_s}{\lambda}\right)}{\kappa\left[\exp\left(\frac{\kappa l_s}{\lambda}\right) + \exp\left(-\frac{\kappa l_s}{\lambda}\right)\right] + \lambda\eta\left[\exp\left(\frac{\kappa l_s}{\lambda}\right) - \exp\left(-\frac{\kappa l_s}{\lambda}\right)\right]} \quad (27)$$

and the transfer function is given by

$$F_T(0, \omega) = A(\omega)\left[\exp\left(\frac{\kappa}{\lambda}l_s\right) - \exp\left(-\frac{\kappa}{\lambda}l_s\right)\right] + \exp\left(-\frac{\kappa}{\lambda}l_s\right). \quad (28)$$

Finally, we have

$$Z_3 = Z_{3a} + \frac{R_m(i\omega C_m R_{sc} + 1)}{i\omega C_m(R_{sc} + R_m) + 1}, \quad (29)$$

where Z_{3a} is the plasma resistance in the soma. κ equals κ_s or κ_{ext} according to the cable model considered.

REFERENCES

1. Rall, W. 1995. The Theoretical Foundation of Dendritic Function. I. Segev, J. Rinzel, and G. M. Shepherd, editors. MIT Press, Cambridge, MA.

2. Johnston, D., and S. M. Wu. 1995. Foundations of Cellular Neurophysiology. MIT Press, Cambridge MA.

3. Brette, R., M. Rudolph, T. Carnevale, M. Hines, D. Beeman, J. M. Bower, M. Diesmann, A. Morrison, P. H. Goodman, F. C. Harris, Jr., M. Zirpe, T. Natschlager, D. Pecevski, B. Ermentrout, M. Djurfeldt, A. Lansner, O. Rochel, T. Vieville, E. Muller, A. Davison, S. El Boustani, and A. Destexhe. 2007. Simulation of networks of spiking neurons: a review of tools and strategies. *J. Comput. Neurosci.* In press. (Article available at http://arxiv.org/abs/q-bio.NC/0611089.).

4. Destexhe, A., M. Rudolph, and D. Paré. 2003. The high-conductance state of neocortical neurons *in vivo*. *Nat. Rev. Neurosci.* 4:739–751.

5. Diba, K., H. A. Lester, and C. Koch. 2004. Intrinsic noise in cultured hippocampal neurons: experiment and modeling. *J. Neurosci.* 24:9723–9733.

6. Jacobson, G. A., K. Diba, A. Yaron-Jakoubovitch, C. Koch, I. Segev, and Y. Yarom. 2005. Subthreshold voltage noise of rat neocortical pyramidal neurones. *J. Physiol.* 564:145–160.

7. Rudolph, M., J. G. Pelletier, D. Paré, and A. Destexhe. 2005. Characterization of synaptic conductances and integrative properties during electrically-induced EEG-activated states in neocortical neurons in vivo. *J. Neurophysiol.* 94:2805–2821.

8. Destexhe, A., and M. Rudolph. 2004. Extracting information from the power spectrum of synaptic noise. *J. Comput. Neurosci.* 17:327–345.

9. Cole, K. S., and R. H. Cole. 1941. Dispersion and absorption in dielectrics. I. Alternating current characteristics. *J. Chem. Phys.* 9:341–351.

10. White, S. N. 1970. A study of lipid bilayer membrane stability using precise measurements of specific capacitance. *Biophys. J.* 10:1127–1148.

11. Eisenberg, R. S., and R. T. Mathias. 1980. Structural analysis of electrical properties. *Crit. Rev. Bioeng.* 4:203–232.

12. Alberts, B., A. Johnson, J. Lewis, M. Raff, K. Roberts, and P. Walter. 2002. Molecular Biology of the Cell, 4th Ed. Garland Publishing, New York.

13. Destexhe, A. and C. Bedard. 2007. A nonideal cable formalism which accounts for fractional power-law frequency scaling of membrane potential activity of cortical neurons. *Soc. Neurosci. Abstr.* 33:251.14.

14. Contreras, D., A. Destexhe, and M. Steriade. 1997. Intracellular and computational characterization of the intracortical inhibitory control of synchronized thalamic inputs *in vivo*. *J. Neurophysiol.* 78:335–350.

15. Douglas, R. J., K. A. Martin, and D. Whitteridge. 1991. An intracellular analysis of the visual responses of neurones in cat visual cortex. *J. Physiol.* 440:659–696.

16. Hines, M. L., and N. T. Carnevale. 1997. The NEURON simulation environment. *Neural Comput.* 9:1179–1209.

17. Destexhe, A., and D. Paré. 1999. Impact of network activity on the integrative properties of neocortical pyramidal neurons in vivo. *J. Neurophysiol.* 81:1531–1547.

18. Bowick, C. 1982. RF Circuit Design. Newnes Elsevier, New York.

19. Alvarez, O., and R. Latorre. 1978. Voltage-dependent capacitance in lipid bilayers made from monolayers. *Biophys. J.* 21:1–17.

20. Raghuram, R. 1990. Computer Simulation of Electronic Circuits. John Wiley & Sons, New York.

21. Raju, G. G. 2003. Dielectrics in Electric Fields. CRC Press, New York.

22. Bedard, C., A. Destexhe, and H. Kroger. 2006. Model of low-pass filtering of local field potentials in brain tissue. *Phys. Rev. E.* 73: 051911.

23. Hanai, T., D. A. Haydon, and J. Taylor. 1965. Some further experiments on bimolecular lipid membranes. *J. Gen. Physiol.* 48(Suppl): 59–63.

24. Marre, O., S. El Boustani, P. Baudot, M. Levy, C. Monier, N. Huguet, M. Pananceau, J. Fournier, A. Destexhe and Y. Frégnac. 2007. Stimulus-dependency of spectral scaling laws in V1 synaptic activity as a read-out of the effective network topology. *Soc. Neurosci. Abstr.* 33:790.6.

25. Ylinen, A., A. Bragin, Z. Nadasdy, G. Jando, I. Szabo, A. Sik, and G. Buzsaki. 1995. Sharp wave-associated high-frequency oscillation (200 Hz) in the intact hippocampus: network and intracellular mechanisms. *J. Neurosci.* 15:30–46.

26. Grenier, F., I. Timofeev, and M. Steriade. 2001. Focal synchronization of ripples (80–200 Hz) in neocortex and their neuronal correlates. *J. Neurophysiol.* 86:1884–1898.